

# A Triplet Mechanism for the Formation of Cyclobutane Pyrimidine Dimers in UV-Irradiated DNA

Ru Bo Zhang and Leif A. Eriksson\*

Department of Natural Sciences and Örebro Life Science Center, Örebro University, 701 82 Örebro, Sweden

Received: January 11, 2006; In Final Form: February 21, 2006

The reaction pathways for the photochemical formation of cyclobutane thymine dimers in DNA are explored using hybrid density functional theory techniques. It is concluded that the thymine–thymine [2 + 2] cycloaddition displays favorable energy barriers and reaction energies in both the triplet and the singlet excited states. The stepwise cycloaddition in the triplet excited state involves the initial formation of a diradical followed by ring closure via singlet–triplet interaction. The triplet mechanism is thus completely different from the concerted singlet state cycloaddition processes. The key geometric features and electron spin densities are also discussed. Bulk solvation has a major effect by reducing the barriers and increasing the diradical stabilities. The present results provide a rationale for the faster cycloreaction observed in the singlet excited states than in the triplet excited states.

## 1. Introduction

Cyclobutane pyrimidine dimers (CPDs) are the major photoproducts observed in UV-irradiated DNA and have been correlated with cell lethality, mutagenesis, and the development of skin cancer.<sup>1,2</sup> CPDs are formed between adjacent pyrimidine bases in DNA exposed to radiation in the far-UV (200–300 nm) range.<sup>3,4</sup> The deleterious effects associated with these lesions largely result from the inhibition of DNA replication and transcription, and perturbation of interstrand base-pairing interactions subsequently leading to miscoding during DNA replication. To specifically recognize and repair these damages, organisms make use of a number of different enzymatic pathways. DNA photolyases, which are activated by concurrent or subsequent exposure to near-UV and visible light (300–500 nm), catalyze the cleavage of the C5–C5' and C6–C6'  $\sigma$ -bonds of a CPD, thereby restoring the pyrimidines to their native states.<sup>5</sup> According to the commonly accepted model, the splitting of the dimer is a consequence of electron transfer from a catalytic cofactor to the dimer.<sup>5–7</sup> The actual mechanisms of action of the different DNA repair enzymes involved in the protection against UV-induced DNA damages have likewise been extensively studied. The splitting of CPD radicals has, for example, been the subject of many quantum chemical studies focused on establishing the most probable direction of electron transfer in the catalytic process.<sup>8–13</sup> Repair of CPD-containing DNA may also occur by base- or nucleotide-excision pathways that involve removal and replacement rather than covalent modifications of the damaged parts.<sup>14</sup>

UV absorption of nucleic acids initially produce localized singlet excited states with high photostability. The ultrafast internal conversion channel has been estimated by measuring fluorescence lifetimes<sup>15</sup> and through computational studies,<sup>16</sup> revealing the behavior of DNA self-protection from photoinduced lesions. Along the internal conversion of singlet excited states, low-lying triplet excited states can become populated by an intersystem crossing (ISC) mechanism. Electron impact

studies have revealed new transitions in thymine and 5-bromouracil, which were assigned to the lowest-lying triplet. The transition of thymine, located at 3.6 eV, was also identified in theoretical studies.<sup>17,18</sup> Despite the fact that triplet formation has a low quantum yield, the longer-lived triplet states are considered to play a potential role for DNA mutants. Hobza et al.<sup>19</sup> proposed that the mutagenic mechanism of A–T to G–C transition, induced by 5-halo-uracils, should proceed on the triplet excited-state potential energy surface (PES) rather than on the singlet ground-state PES. The hypothesis was based on correlated quantum chemical calculations, and is supported by related studies.<sup>20</sup>

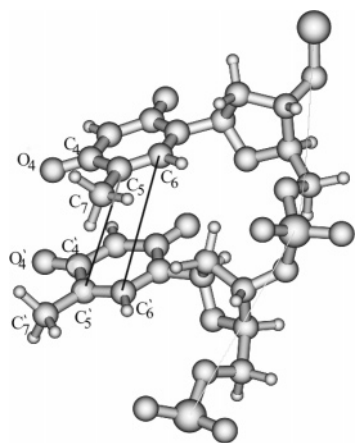
The role of triplet excited states in DNA on the formation of CPDs was first suggested by Cadet et al.<sup>21</sup> The formation of CPDs might, however, also occur on the singlet excited-state PES. In our recent studies of photochemical [2 + 2] cycloadditions, leading to the formation of different CPDs in UV-irradiated DNA, we have explored the concerted singlet excited-state reactions between thymines (T $\diamond$ T), cytosines (C $\diamond$ C), uracils (U $\diamond$ U), cytosine and thymine (C $\diamond$ T), and 5-methylcytosine (5mC $\diamond$ 5mC).<sup>22</sup> On the basis of the topology of the S<sub>1</sub> surfaces, the investigations were able to explain the observation that the CPDs formed between thymine bases (T $\diamond$ T) are much more common than the other ones.

More recent studies showed time-resolved CPD formation for the first time by recording the absorption band of (dT)<sub>20</sub> for 200 ns.<sup>23</sup> The absence of triplet absorption resulted in an uncertainty as to whether CPD is formed via singlet or triplet excited states even though the authors believe that triplet formation does indeed occur in the oligonucleotide solution at 200 ns. The aim of the present study is to elucidate by theoretical means the mechanism of CPD formation on the lowest-lying triplet excited-state surface and the interaction between the lowest-lying triplet and singlet states. We also hope that the present work will contribute to further studies on the mechanism of CPD formation.

The following notation is employed throughout the work: TT represents the thymine–thymine systems, subscripts S and T

\* Author to whom correspondence should be addressed.  
E-mail: leif.eriksson@nat.oru.se.

## SCHEME 1



are used to specify the state, and the number in superscript is a running index relating to the PES (e.g.,  $TT_S^2$ ,  $TT_T^5$ , and so forth).

## 2. Computational Methods

Photoinduced dimerization reactions of large molecular aggregates are a major challenge for theoretical studies. The most appropriate approach in this context is to calculate the PES using a multireference approach such as complete active space second-order perturbation (CASPT2) theory<sup>24</sup> to account for both dynamical electron correlation and near-degeneracy effects. Because of the computational requirements associated with such an approach, most quantum chemical investigations of photocycloadditions have, however, been carried out at the complete active space self-consistent field (CASSCF)<sup>25</sup> level of theory and have primarily concerned photocycloadditions involving small alkenes or dienes.<sup>26–31</sup> However, density functional theory (DFT)-based methods have made it possible to explore photocycloadditions in larger systems (such as current nucleoside dimers) using quantum chemical calculations, even though DFT in comparison with multiconfigurational ab initio theory in certain regards constitutes a less appropriate foundation for the modeling of photochemical reaction processes. The approximate density functionals used in current formulations of Kohn–Sham single-reference DFT may, for example, fail to describe systems in which near degeneracies are occurring between different electronic configurations. Our earlier time-dependent (TD)-DFT calculations<sup>22a,b</sup> yielded an approximate potential energy curve for the concerted singlet-state photochemical reaction pathway having a minimum (a “potential well”) at a nuclear configuration corresponding to that of the transition structure along the thermal reaction path, in accordance with the van der Lugt and Oosterhoff model of photochemical reactions.<sup>32</sup>

In this paper, we have explored the possible triplet energy pathways to dimerization, assuming the system to undergo intersystem crossing after initial excitation to  $S_1$  (or  $S_2$ ). All triplet calculations were carried out using the B3LYP hybrid density functional<sup>33–35</sup> as implemented in the Gaussian 03 suite of programs in conjunction with the 6-31G(d,p) and 6-311++G-(d,p) basis sets.<sup>36</sup> The computational model system is focused on the formation of the biologically relevant *cis-syn* stereoisomer (cf. Scheme 1). The neglect of the influence of the DNA backbone (e.g., strain effects) and the complementary strand (e.g., hydrogen-bonded interactions) on the reacting bases is necessitated by the need to calculate numerous structures (see below) through which the systems pass on the route between reactants and products. Even though the surrounding DNA and

the presence of a solvent most certainly affect the photodimerization, it may be noted that the absorption of light by DNA results in localization of energy primarily at the sites of the bases.

For the reactant complexes, unconstrained geometry optimizations lead to coplanar structures in which the bases interact by hydrogen bonds. As this is clearly an unphysical model of neighboring bases in DNA, we chose to optimize the reactant complexes with geometrical constraints ( $T + T$ ,  $R(C5-C5') = 4.18 \text{ \AA}$ ,  $R(C6-C6') = 4.46 \text{ \AA}$ , and  $C7-C5-C5'-C7' = 35.3^\circ$ ) to ensure a structure as in native DNA. No geometrical constraints were however enforced when optimizing transition structures or products. B3LYP/6-31G(d,p) frequency calculations were performed to identify the stationary points as either minima (reactant complexes and product structures) or first-order saddle points (transition structures) and to extract zero-point vibrational energy (ZPE) corrections. Bulk solvation effects were considered using the integral electron formalism of the polarized continuum model (IEF-PCM).<sup>37</sup> In parallel, the calculations were also performed on the singlet states using the same geometric conformations. The correlated photochemical reaction pathways of the cycloadditions were explored on the basis of TD-DFT calculations developed by Scuseria and co-workers.<sup>38</sup> This implementation computes vertical excitation energies only. In principle, this prevents the exact localization of stationary points on an excited-state potential energy surface. However, within the framework of the van der Lugt and Oosterhoff model<sup>32</sup> in which the geometrical features of the excited-state path are similar to those of the ground-state path, an approximate excited-state potential energy surface can be calculated using ground-state geometries.

## 3. Results and Discussions

**3.1. Cycloaddition on Singlet PES.** First, the cycloaddition reactions on the singlet ground and excited states are briefly reviewed. The optimized singlet ground-state geometries of the initial complex ( $TT_S^1$ ), transition state ( $TT_S^2$ ), and cross-linked product ( $TT_S^3$ ), and the relevant geometric parameters, are shown in Figure 1.

For the initial complex ( $TT_S^1$ ), the highest occupied molecular orbital (HOMO) and lowest unoccupied molecular orbital (LUMO), respectively, are mainly localized on each of the two bases, with an energy gap of 0.44 au. The stabilization energy of the complex  $TT_S^1$ , relative to two isolated thymine bases, is  $2.3 \text{ kcal mol}^{-1}$  at the B3LYP/6-31G(d,p) level. Along the concerted thermal path, the  $TT_S^2$  transition structure is associated with a barrier of  $87.6 \text{ kcal mol}^{-1}$ . The  $C5 \cdots C5'$  distance is  $0.2 \text{ \AA}$  longer than the  $C6 \cdots C6'$  one, which is attributed to the repulsion between the two methyl groups. In the  $TT_S^2$  transition structure, puckering of the thymine moieties is furthermore observed, due to the conversion of the  $C5-C6$  double bonds to single bonds. The  $\angle C5-C6-C6'-C5'$  dihedral angle is  $18.1^\circ$ . In the produced CPD, the individual  $C5C6$  features are typical to those of single bonds and with distances ca.  $0.2 \text{ \AA}$  greater than those of the initial complex. The  $\angle C5-C6-C6'-C5'$  dihedral angle is  $19.9^\circ$ . In comparison with the X-ray crystal structure of the TT dimer in decamer DNA,<sup>39</sup> given in parentheses of Figure 1, we note that the  $C5C6$  and  $C5'C6'$  bonds in the crystal data are essentially still  $\pi$ -bonds ( $1.3\text{--}1.4 \text{ \AA}$ ), whereas upon cycloaddition they should attain a complete  $\sigma$ -character. The low resolution ( $2.5 \text{ \AA}$ ) of the X-ray data may be a possible explanation for this. The bridging  $C5-C5'$  and  $C6-C6'$  distances are in good agreement between experiment and theory.

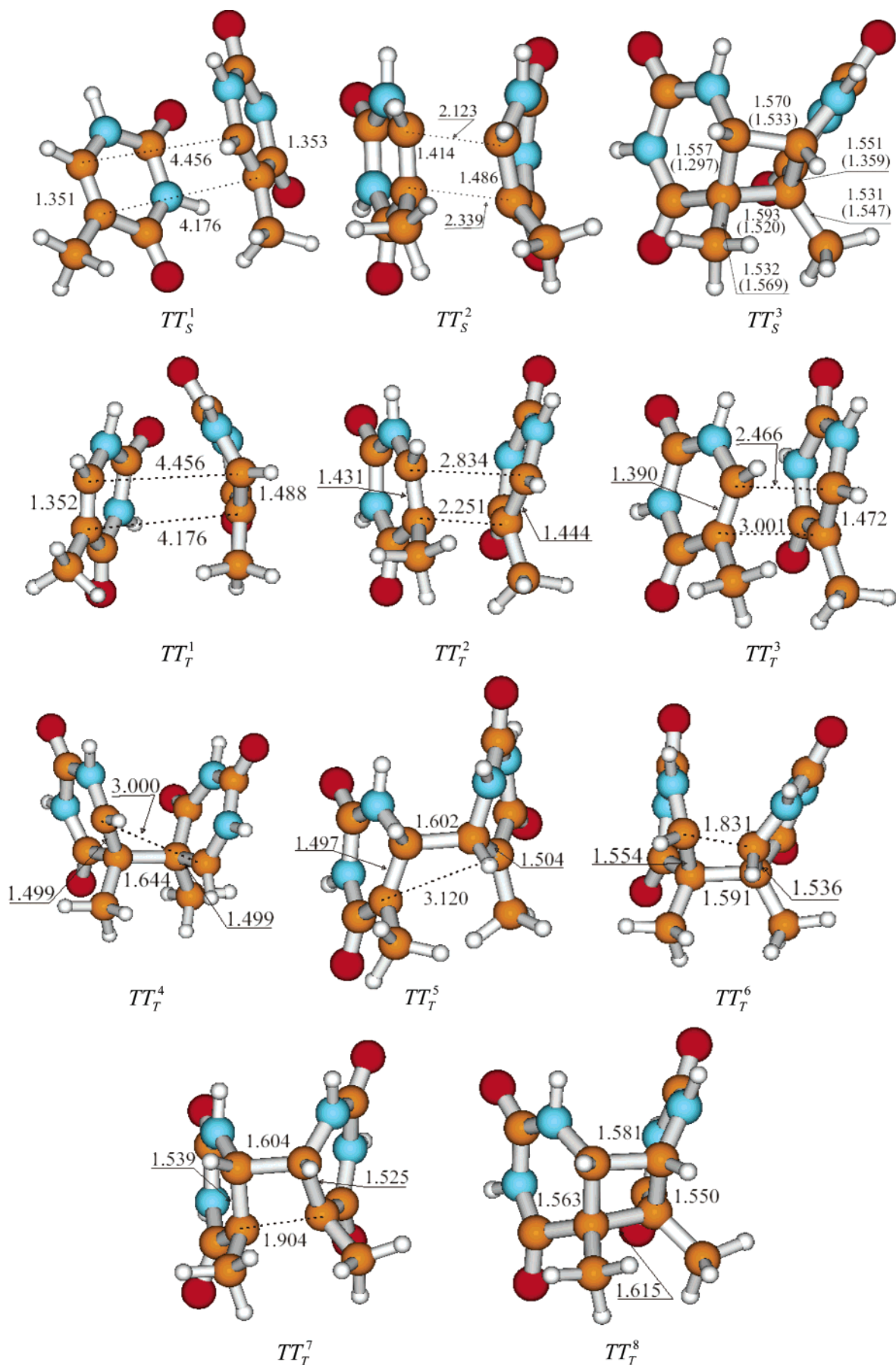


**Figure 1.** Selected UB3LYP/6-31G(d,p) geometrical parameters of the stationary structures along the thymine-thymine cycloaddition reaction in their singlet and lowest-lying triplet states. For the singlet CPD product  $TT_S^3$  X-ray data from PDB entry 1N4E<sup>39</sup> is added in parentheses.



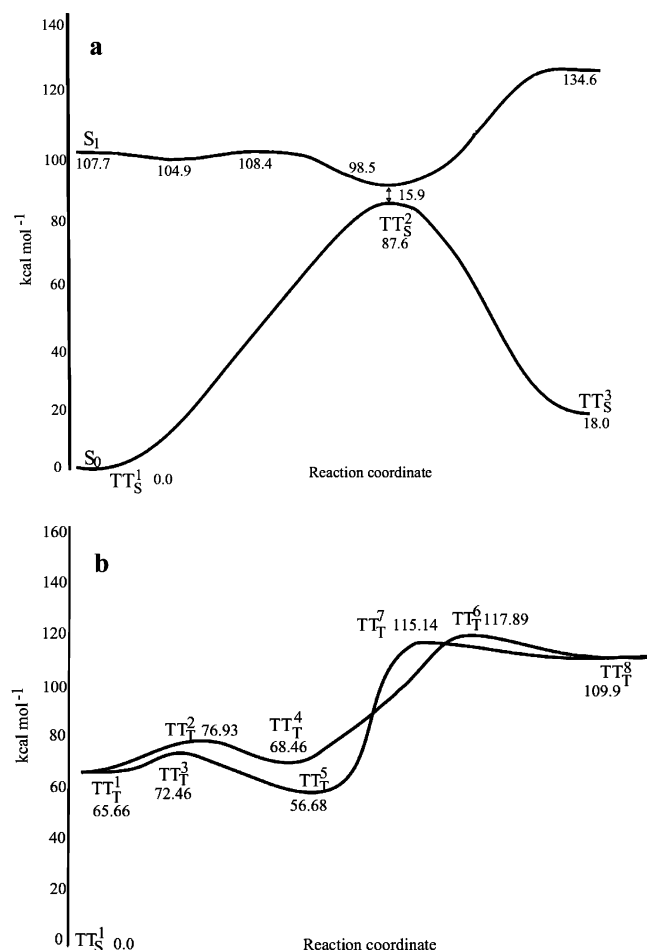


**Figure 2.** Energy curves for thermal and photochemical cycloaddition reactions of two thymines (B3LYP/6-31G(d,p) level; kcal mol<sup>-1</sup>): (a) singlet state; (b) triplet state.

**TABLE 1: Relative Energies<sup>a</sup> (without ZPE Corrections), in kcal mol<sup>-1</sup>, of the Species along the Thymine–Thymine Cycloaddition Reactions**

B3LYP/ 6-31G(d,p)		B3LYP/ 6-31G(d,p)		B3LYP/ 6-311++G(d,p)		
vacuum		vacuum	ε = 4.3	vacuum	ε = 4.3	
TT <sub>S</sub> <sup>1</sup> <sup>a</sup>	0.0	TT <sub>T</sub> <sup>1</sup>	65.7	69.5	65.9	67.9
TT <sub>S</sub> <sup>2</sup>	87.6	TT <sub>T</sub> <sup>2</sup>	76.9	75.5	76.2	74.9
TT <sub>S</sub> <sup>3</sup>	18.0	TT <sub>T</sub> <sup>3</sup>	72.5	70.5	71.2	69.2
		TT <sub>T</sub> <sup>4</sup>	68.5	68.4	69.4	69.0
		TT <sub>T</sub> <sup>5</sup>	56.7	56.6	57.1	54.4
		TT <sub>T</sub> <sup>6</sup>	117.9	114.8	119.7	112.2
		TT <sub>T</sub> <sup>7</sup>	115.1	115.1	116.8	113.8
		TT <sub>T</sub> <sup>8</sup>	109.9	110.3	112.2	109.8

<sup>a</sup> The energy of TT<sub>s</sub><sup>1</sup> used as zero in the table is -908.301467 au (for vacuum) and -908.330264 au (for  $\epsilon = 4.3$ ) at the B3LYP/6-31G(d,p) level and -908.551203 au (vacuum) and -908.569890 au ( $\epsilon = 4.3$ ) at the B3LYP/6-311++G(d,p) level.

The potential energy curves of the thermal and photochemical singlet reaction pathways are presented in Figure 2a; relative energies are given in Table 1. The total reaction energy is 18.0 kcal mol<sup>-1</sup>. Both the high barrier and endothermicity illustrate that thermally induced CPD formation is energetically inaccessible. The singlet photochemical process (S<sub>1</sub> surface) of CPD formation reveals an energy barrier of only 3–4 kcal mol<sup>-1</sup> before the system reaches the potential well from which it decays to the ground-state surface. As mentioned above, the excited singlet route to the formation of CPDs has recently been verified by time-resolved experiments.<sup>23</sup>

**TABLE 2: Mulliken Spin Densities (e<sup>-</sup>; B3LYP/6-31G(d,p) Level) of Selected Atoms in Each Species along the Triplet Thymine–Thymine Cycloaddition Reactions**

	C4	O4	C5	C6	C4'	O4'	C5'	C6'
TT <sub>t</sub> <sup>1</sup>	0	0	0	0	-0.049	0.231	0.751	0.817
TT <sub>t</sub> <sup>2</sup>	-0.006	0.069	0.176	0.578	-0.008	0.047	0.239	0.068
TT <sub>t</sub> <sup>3</sup>	0.014	0.088	-0.017	0.047	-0.046	0.190	0.663	0.518
TT <sub>t</sub> <sup>4</sup>	0.006	0.011	-0.004	0.843	0.001	0.003	-0.008	0.841
TT <sub>t</sub> <sup>5</sup>	-0.079	0.179	0.830	-0.020	-0.083	0.189	0.843	-0.015
TT <sub>t</sub> <sup>6</sup>	0.427	0.587	0.011	0.135	0.038	0.022	0.084	0.190
TT <sub>t</sub> <sup>7</sup>	0.431	0.862	0.031	0.036	0.011	0.039	0.319	0.016
TT <sub>t</sub> <sup>8</sup>	0.670	0.993	0.049	0.025	-0.001	0.010	0.056	0.006

**3.2. Cycloaddition on the Lowest-Lying Triplet Excited PES.** As noted in earlier studies,<sup>18,40</sup> the main structural feature of the lowest-lying triplet of pyrimidine bases is the conversion of the C5–C6  $\pi$ -bond (1.352 Å) to a  $\sigma$ -bond (1.501 Å). For the isolated thymine base, the singlet–triplet adiabatic energy gap is 65.0 kcal mol<sup>-1</sup> at the B3LYP/6-31G(d,p) level. The spin densities are localized on the reactive C5 and C6 atoms. The electronic features imply that the cycloaddition mechanism on the triplet PES should be different from the one on the singlet surface.

The first excited triplet, TT<sub>t</sub><sup>1</sup>, can be reached via ISC from the excited singlet surface. The optimized lowest-lying triplet stationary points are shown in Figure 1. In the initial triplet complex TT<sub>t</sub><sup>1</sup>, the C5C6 distance of one fragment of TT<sub>t</sub><sup>1</sup> is the same as for the singlet thymine base, showing that it retains the properties of the singlet ground state. The C5C6 distance of the other unit is 1.488 Å, which is close to the length formed in the triplet thymine base. A dramatic puckering structure is observed for this fragment, and the H(C6') deviates considerably from the quasi-plane. The unpaired spin densities are mainly localized on C6' (0.82 electrons) and C5' (0.75 electrons), as seen in Table 2. The stabilization energy of the TT<sub>t</sub><sup>1</sup> complex is 4.2 kcal mol<sup>-1</sup>, relative to the energetic sum of isolated triplet and singlet bases, which is slightly higher than the stabilization energy of the singlet ground-state complex TT<sub>s</sub><sup>1</sup> compared to two singlet molecules. The adiabatic singlet–triplet energy gap between TT<sub>s</sub><sup>1</sup> and TT<sub>t</sub><sup>1</sup> is 65.7 kcal mol<sup>-1</sup>, which is very close to the single base case.

The reaction energy profiles of triplet cycloaddition reactions are presented in Figure 2b. One of the paths to the formation of cis–syn CPDs on the triplet PES proceeds through initial attack by C5 on C5', followed by C6–C6' cross-link formation (route TT<sub>t</sub><sup>1</sup>–TT<sub>t</sub><sup>2</sup>–TT<sub>t</sub><sup>4</sup>–TT<sub>t</sub><sup>6</sup>–TT<sub>t</sub><sup>8</sup>). From TT<sub>t</sub><sup>1</sup> to TT<sub>t</sub><sup>2</sup>, the activation energy is 11.3 kcal mol<sup>-1</sup> at the B3LYP/6-31G(d,p) level (10.3 kcal mol<sup>-1</sup> at the B3LYP/6-311++G(d,p) level). In the transition structure the base puckering is lost, and repulsion between the two methyl groups makes these deviate from the individual base planes. The C5...C5' distance is 2.251 Å, which is slightly shorter than that in TT<sub>s</sub><sup>2</sup>. The C6...C6' distance is 2.834 Å, and the two unpaired electrons are now more delocalized over both fragments, indicative of spin transfer from one base to the other. The  $\angle$ C5–C6–C6'–C5' dihedral angle is 27.1°; i.e., the two bases are now ca. 8° less rotated relative to each other, compared to the situation in native DNA (dihedral angle 35.3°). The resulting C5–C5' cross-linked intermediate TT<sub>t</sub><sup>4</sup> is a diradical with spin densities localized to C6 and C6' (0.84 e<sup>-</sup> on each). The  $\angle$ C5–C6–C6'–C5' dihedral angle is now 33.9°. The reaction energy relative to TT<sub>t</sub><sup>1</sup> is +2.8 (+3.5) kcal mol<sup>-1</sup> at the B3LYP/6-31G(d,p) (B3LYP/6-311++G(d,p)) level. The energetic difference between TT<sub>t</sub><sup>2</sup> and TT<sub>t</sub><sup>4</sup> is -8.5 (-6.8) kcal mol<sup>-1</sup>.

From the intermediate TT<sub>t</sub><sup>4</sup> to the transition structure for ring closure on the triplet surface, TT<sub>t</sub><sup>6</sup>, 49.4 kcal mol<sup>-1</sup> must be

added at the B3LYP/6-31G(d,p) level. The result is little influenced by additional polarization or diffuse basis functions. The H atoms attached to C6 and C6' in the transition structure  $TT_T^6$  deviate from the individual plane with dihedral angles  $\angle H6-N1-C5-C6 = -23.2^\circ$  and  $\angle H6'-N1'-C5'-C6' = -24.9^\circ$ , respectively. The  $\angle C5-C6-C6'-C5'$  dihedral angle is reduced to  $14.8^\circ$ , and the density is mainly located on C4–O4 of one base. The energetic difference between  $TT_T^6$  and  $TT_T^8$ , the final CPD triplet-state product, is  $-8.0$  ( $-7.5$ ) kcal mol $^{-1}$ . For  $TT_T^8$ , the C5C5' and C6C6' bond lengths are 1.615 and 1.581 Å, respectively, slightly longer than the corresponding distances in the singlet ground-state cycloadduct  $TT_S^3$ , and the C5C6 and C5'C6' bond lengths are 1.563 and 1.550 Å, respectively, which are almost consistent with the ones in  $TT_S^3$ . The unpaired spin electrons in  $TT_T^8$  are localized on C4 (0.67 e $^-$ ) and O4 (0.99 e $^-$ ) of one base, similar to the case of  $TT_T^6$ . It is noteworthy that the singlet–triplet adiabatic energy gap between  $TT_S^3$  and  $TT_T^8$  is 92.0 kcal mol $^{-1}$  at the B3LYP/6-31G(d,p) level, i.e., considerably higher than for the initial reactants  $TT_S^1$  and  $TT_T^1$ .

The other pathway leading to the formation of cis–syn CPD on the triplet PES is by initial C6 attack to C6' followed by subsequent formation of the C5–C5' cross-link. Along the  $TT_T^1$ – $TT_T^3$ – $TT_T^5$ – $TT_T^7$ – $TT_T^8$  route, an initial barrier of 6.8 kcal mol $^{-1}$  must be overcome at the B3LYP/6-31G(d,p) level (5.3 kcal mol $^{-1}$  at the B3LYP/6-311++G(d,p) level) to reach  $TT_T^5$ , which is lower than the one leading from  $TT_T^1$  to  $TT_T^4$ . In the transition structure  $TT_T^3$ , the C6...C6' and C5...C5' distances are 2.466 and 3.001 Å, respectively, and the  $\angle C5-C6-C6'-C5'$  dihedral angle is  $27.2^\circ$ . Spin densities are mainly found on C5' and C6' but are starting to delocalize over both moieties. The  $TT_T^5$  intermediate is also a diradical with a C6C6' bond length of 1.602 Å, which is slightly shorter than the C5C5' distance in  $TT_T^4$ . The C5...C5' distance is 3.120 Å and the  $\angle C5-C6-C6'-C5'$  dihedral angle is  $60.8^\circ$ . Spin densities are, as expected, located on C5 and C5' (ca 0.84 e $^-$  on each). The  $TT_T^5$  diradical is more stable than  $TT_T^4$  by 11.8 (12.3) kcal mol $^{-1}$ . The reaction energy for  $TT_T^1 \rightarrow TT_T^5$  is  $-9.0$  kcal mol $^{-1}$  at the B3LYP/6-31G(d,p) level. Thus, the initial cross-link reaction  $TT_T^1 \rightarrow TT_T^5$  (formation of the C6–C6' bond) is preferred over  $TT_T^1 \rightarrow TT_T^4$  (formation of the C5–C5' bond), primarily due to reduced steric repulsion between the C5 methyl groups in  $TT_T^3$  compared with  $TT_T^2$ . From  $TT_T^5$  to  $TT_T^7$ , the activation energy is 58.5 (68.5) kcal mol $^{-1}$ , which is comparable to the barrier for the reaction  $TT_T^4 \rightarrow TT_T^6$ . For the transition structure  $TT_T^7$ , the C5...C5' distance is 1.904 Å, and C6...C6' is nearly unchanged compared to the distance in  $TT_T^5$ . The  $\angle C5-C6-C6'-C5'$  dihedral angle is  $20.6^\circ$ . The energy difference between  $TT_T^7$  and  $TT_T^8$  is  $-5.2$  ( $-4.6$ ) kcal mol $^{-1}$ .

According to the above results, the T $\odot$ T dimer cannot be formed on the triplet PES only, due to the high barriers for both the  $TT_T^4 \rightarrow TT_T^6 \rightarrow TT_T^8$  and  $TT_T^5 \rightarrow TT_T^7 \rightarrow TT_T^8$  reactions. The present results hence do not agree fully with the results implied by various experiments that the T $\odot$ T dimer can potentially be formed through the triplet excited state alone.<sup>41</sup> Instead, knowledge of the interaction between the lowest-lying triplet and the singlet ground-state surface is important for an understanding of the triplet CPD formation.

To obtain a reliable singlet–triplet interaction profile, the PES was scanned from  $TT_T^4$  to  $TT_T^6$  by varying the C6...C6' distances with a step length of 0.1 Å, constraining the C5–C5' distance at 1.644 Å and optimizing the remaining coordinates.

The same procedure was used to determine the PES from  $TT_T^5$  to  $TT_T^7$ , fixing C6–C6' at 1.602 Å and scanning the C5...C5' distance.

The energies for the singlet/triplet scans are displayed in Figure 3a (starting from  $TT_T^4$ ) and 3b (starting from  $TT_T^5$ ). For system  $TT_T^4$ , with C5–C5' already formed, there is a triplet–singlet crossing point at the C6...C6' distance of 2.335 Å with an energy of ca.  $-908.169952$  au at the B3LYP/6-31G(d,p) level. Thus the estimated energy gap from  $TT_T^4$  to the crossing point is approximately 14.1 kcal mol $^{-1}$ . For the path  $TT_T^5$  to  $TT_T^7$  (Figure 3b), the C5...C5' distance at the crossing point is close to 2.397 Å, and the energy gap from the initial  $TT_T^5$  complex to the crossing point is estimated to be 14.9 kcal mol $^{-1}$ . The determined energy barriers to the spin crossover points are dramatically lower than the 87.6 kcal mol $^{-1}$  barrier for the thermal cycloaddition reaction and the ca. 50 kcal mol $^{-1}$  required to reach the triplet CPD, indicating that the triplet state is a possible channel to the formation of the T $\odot$ T dimer if interaction with the singlet surface is considered after formation of the initial single cross-linked diradical intermediate.

**3.3. Effects of Bulk Solvation.** In this section, we will address the role of bulk solvation on the reaction profiles. The dielectric constant  $\epsilon = 4.3$  is used to simulate the local surroundings of DNA. In Table 1, the energetics derived from the density functional theory self-consistent reaction field (DFT-SCRF) calculations are listed. Several features can be observed from the reaction profiles after accounting for the implicit solvent effect generated by the nonaqueous medium. Relative to the gas-phase value, the stability of  $TT_S^1$  is enhanced by 18.1 kcal mol $^{-1}$  due to bulk solvation effects. The barrier heights decrease in the  $TT_T^1 \rightarrow TT_T^2$  and  $TT_T^1 \rightarrow TT_T^3$  reaction steps to 6.0 and 1.1 kcal mol $^{-1}$ , respectively, compared to the corresponding gas-phase values of 11.3 and 6.8 kcal mol $^{-1}$  at the B3LYP/6-31G(d,p) level. Essentially the same result is obtained when the larger basis set is considered. The reaction energies for the formation of the diradicals, for example,  $TT_T^1 \rightarrow TT_T^4$  and  $TT_T^1 \rightarrow TT_T^5$ , are  $-1.1$  and  $-12.9$  kcal mol $^{-1}$  at the B3LYP/6-31G(d,p) level (gas-phase values of  $+2.8$  and  $-9.0$  kcal mol $^{-1}$ , respectively). The bulk effects of the surroundings even at such a low value of  $\epsilon$  as 4.3 D are hence considerable, some 4–6 kcal/mol on both reaction rates (barrier heights) and stabilities of the two diradical intermediates.

DFT-SCRF is also used to study the bulk solvent effects on the interaction between singlet and triplet states. As seen in Figure 3, the sites of the crossing points are essentially unchanged by the influence of bulk solvent, although their stabilities are enhanced. The energy gaps from the crossing points to the initial  $TT_T^4$  and  $TT_T^5$  complexes are estimated to 13.2 and 14.3 kcal mol $^{-1}$ , respectively, which are slightly lower than the corresponding gas-phase values.

## 4. Conclusions

In the present work, hybrid DFT methods have been employed to investigate the processes of CPD formation on the singlet and lowest-lying triplet excited states with the objective to determine reaction energy profiles. Geometries, unpaired electron spin densities, and reaction energies were obtained at the B3LYP/6-31G(d,p) level in the gas phase, followed by energy calculations performed at the same level in solution ( $\epsilon = 4.3$ ) using the IEF-PCM model. Single-point calculations were also performed, both in vacuo and in bulk solvent, using the larger 6-311++G(d,p) basis set. Two stepwise pathways to CPD formation are found on the triplet PES, and the results are compared to the concerted mechanism of formation on the

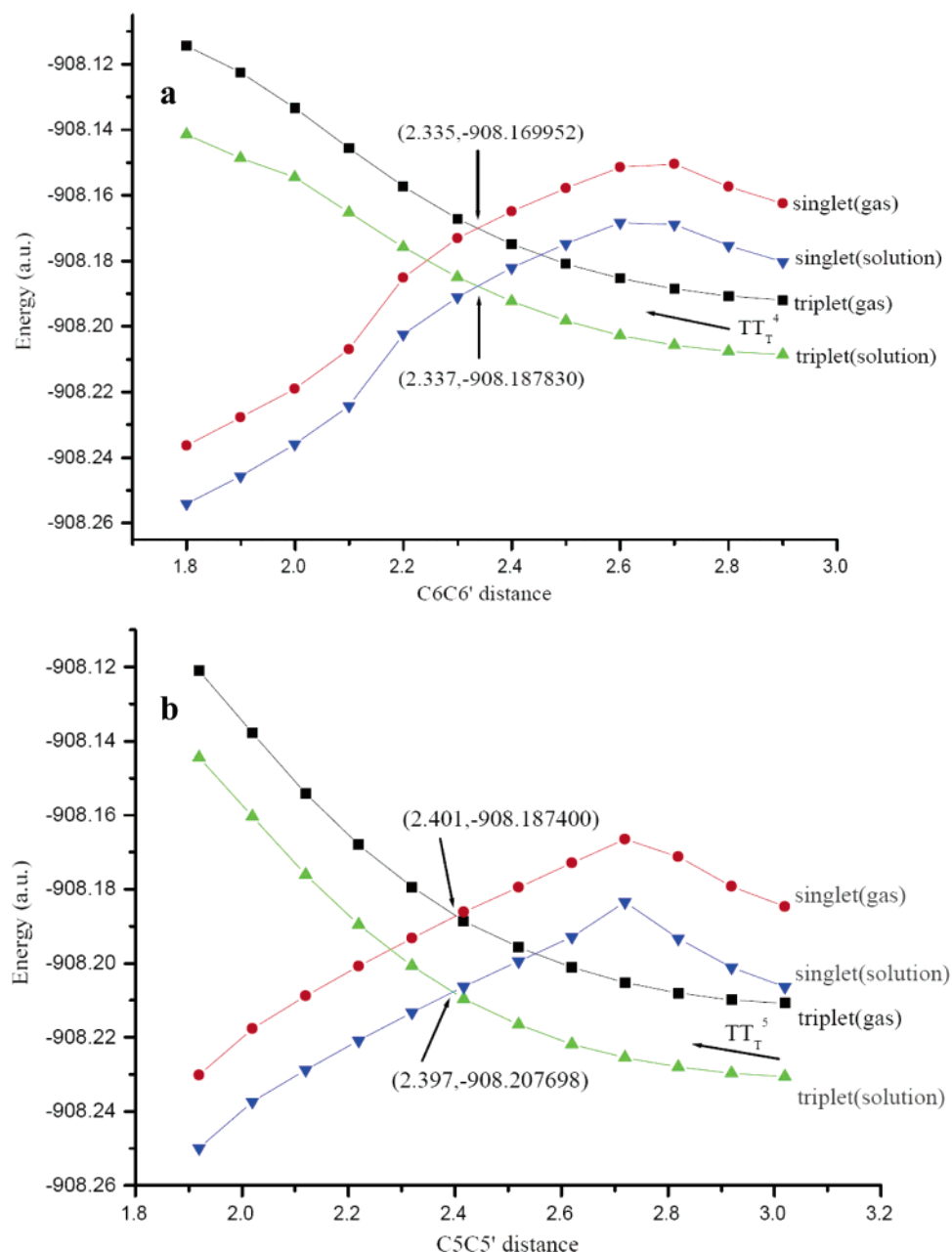


**Figure 3.** Interaction curves for singlet and triplet states along the path from diradical intermediates to fully cross-linked CPD, obtained at the B3LYP/6-31G(d,p) level: (a) from right to left, moving in the direction  $TT_T^4$  toward  $TT_T^6$ ; (b) from right to left, moving in the direction  $TT_T^5$  toward  $TT_T^7$ .

singlet surface. For the initial reactions (formation of the first C–C' cross-link bond, either C5–C5' or C6–C6') on the triplet PES in gas phase, the barriers for the two paths are between 6 and 11.5 kcal mol<sup>-1</sup> and result in the formation of diradical intermediates. The energetically most favorable path, both in terms of activation energy and diradical stability, is that initiated by formation of the C6–C6' bond ( $TT_T^5$  intermediate), as compared with the formation of  $TT_T^4$  (the C5–C5' cross-linked intermediate) in which the methyl groups on C5 and C5' present unfavorable interactions.

The reactions from the diradicals to the ring-closed CPDs are prohibited by high energetic barriers, comparable to the one of the thermal singlet ground-state process. Instead, the interaction between triplet and singlet states close to the diradical intermediates plays a significant role in the CPD formation. Our estimated energy differences from the two diradicals to the corresponding singlet–triplet crossing points range from 14 to

15 kcal mol<sup>-1</sup> and may pose a possible channel for CPD formation via the triplet PES. Bulk solvation effects lead to a dramatic decrease of the initial energetic barriers and reaction energies, whereas the energy gaps between the diradicals and the singlet–triplet crossing points are little affected.

The current data provide a rationale for the observation that triplet mechanisms may be involved in CPD formation, albeit at a slower rate than on the excited singlet surfaces. A crucial factor in this respect is the possibility for the initially excited singlet system to undergo intersystem crossing to reach the triplet complex  $TT_T^1$ .

**Acknowledgment.** The Swedish Science Research Council (VR) is gratefully acknowledged for financial support. We also acknowledge generous grants of computing time at the National supercomputing facilities in Linköping (NSC) and Stockholm (PDC).

## References and Notes

- (1) Sage, E. *Photochem. Photobiol.* **1993**, 57, 163.
- (2) Pfeifer, G. P. *Photochem. Photobiol.* **1997**, 65, 270.
- (3) Wang, S. Y. *Photochemistry and Photobiology of Nucleic Acids*, Chemistry; Academic Press: San Diego, CA, 1976; Vol. 1.
- (4) Harm, W. *Biological Effects of Ultraviolet Radiation*; Cambridge University Press: Cambridge, U. K., 1984.
- (5) Sancar, A. *Biochemistry* **1994**, 33, 2.
- (6) Heelis, P. F.; Hartman, R. F.; Rose, S. D. *Chem. Soc. Rev.* **1995**, 24, 289.
- (7) Carell, T.; Burgdorf, L. T.; Kundu, L. M.; Cichon, M. *Curr. Opin. Chem. Biol.* **2001**, 5, 491.
- (8) Voityuk, A. A.; Michel-Beyerle, M.-E.; Rosch, N. *J. Am. Chem. Soc.* **1996**, 118, 9750.
- (9) Voityuk, A. A.; Rosch, N. *J. Phys. Chem. A* **1997**, 101, 8335.
- (10) Aida, M.; Inoue, F.; Kaneko, M.; Dupuis, M. *J. Am. Chem. Soc.* **1997**, 119, 12274.
- (11) Rak, J.; Voityuk, A. A.; Rosch, N. *J. Phys. Chem. A* **1998**, 102, 7168.
- (12) Rak, J.; Voityuk, A. A.; Michel-Beyerle, M.-E.; Rosch, N. *J. Phys. Chem. A* **1999**, 103, 3569.
- (13) Durbecq, B.; Eriksson, L. A. *J. Am. Chem. Soc.* **2000**, 122, 10126.
- (14) Sancar, A.; Sancar, G. B. *Annu. Rev. Biochem.* **1988**, 57, 29.
- (15) (a) Crespo-Hernandez, C. E.; Cohen, B.; Hare, P. M.; Kohler, B. *Chem. Rev.* **2004**, 104, 1977. (b) Pecourt, J.-M. L.; Peon, J.; Kohler, B. *J. Am. Chem. Soc.* **2000**, 122, 9348. (c) Pecourt, J.-M. L.; Kohler, B.; Peon, J. *J. Am. Chem. Soc.* **2001**, 123, 5166.
- (16) (a) Sobolewski, A. L.; Domcke, W. *Eur. Phys. J. D* **2002**, 20, 369. (b) Ismail, N.; Blancafort, L.; Olivucci, M.; Kohler, B.; Robb, M. A. *J. Am. Chem. Soc.* **2002**, 124, 6818. (c) Merchan, M.; Serrano-Andres, L. *J. Am. Chem. Soc.* **2003**, 125, 8108. (d) Blancafort, L.; Robb, M. A. *J. Phys. Chem. A* **2004**, 108, 10609. (e) Zgierski, M. Z.; Patchkovskii, S.; Fujiwara, T.; Lim, E. C. *J. Phys. Chem. A* **2005**, 109, 9384. (f) Merchan, M.; Serrano-Andres, L.; Robb, M. A.; Blancafort, L. *J. Am. Chem. Soc.* **2005**, 127, 1820.
- (17) Abouaf, R.; Pommier, J.; Dunet, H. *Chem. Phys. Lett.* **2003**, 381, 486.
- (18) Nguyen, M. T.; Zhang, R.; Nam, P.-C.; Ceulemans, A. *J. Phys. Chem. A* **2004**, 108, 6554.
- (19) Hanus, M.; Kabelac, M.; Nachtigallova, D.; Hobza, P. *Biochemistry* **2005**, 44, 1701.
- (20) Blancafort, L.; Bertran, J.; Sodupe, M. *J. Am. Chem. Soc.* **2004**, 126, 12770.
- (21) Cadet, J.; Vigny, P. In *Bioorganic Photochemistry*; Morrison, H., Ed.; John Wiley & Sons: New York, 1990; pp 1–272.
- (22) (a) Durbecq, B.; Eriksson, L. A. *J. Photochem. Photobiol., A* **2002**, 152, 95. (b) Durbecq, B.; Eriksson, L. A. *Photochem. Photobiol.* **2003**, 78, 159. (c) Li, X. Y.; Eriksson, L. A. *Chem. Phys. Lett.* **2005**, 401, 99.
- (23) Marguet, S.; Markovits, D. *J. Am. Chem. Soc.* **2005**, 127, 5780.
- (24) Andersson, K.; Malmqvist, P.-Å.; Roos, B. O. *J. Chem. Phys.* **1992**, 96, 1218.
- (25) Roos, B. O. The complete active space self-consistent field method and its application in electronic structure calculations. In *Advanced Chemistry and Physics: Ab Initio Methods in Quantum Chemistry, Part II*; Lawley, K. P., Ed.; Wiley: New York, 1987; pp 399–446.
- (26) Bernardi, F.; De S.; Olivucci, M.; Robb, M. A. *J. Am. Chem. Soc.* **1990**, 112, 1737.
- (27) Bernardi, F.; Olivucci, M.; Robb, M. A. *Acc. Chem. Res.* **1990**, 23, 405.
- (28) Bernardi, F.; Bottoni, A.; Olivucci, M.; Venturini, A.; Robb, M. A. *J. Chem. Soc., Faraday Trans.* **1994**, 90, 1617.
- (29) Bearpark, M. J.; Deumal, M.; Robb, M. A.; Vreven, T.; Yamamoto, N.; Olivucci, M.; Bernardi, F. *J. Am. Chem. Soc.* **1997**, 119, 709.
- (30) Wilsey, S.; Gonzalez, L.; Robb, M. A.; Houk, K. N. *J. Am. Chem. Soc.* **2000**, 122, 5866.
- (31) García-Expósito, E.; Bearpark, M. J.; Ortuño, R. M.; Robb, M. A.; Branchadell, V. *J. Org. Chem.* **2002**, 67, 6070.
- (32) van der Lugt, W. T. A. M.; Oosterhoff, L. J. *J. Am. Chem. Soc.* **1969**, 91, 6042.
- (33) Lee, C.; Yang, W.; Parr, R. G. *Phys. Rev. B* **1988**, 37, 785.
- (34) Becke, A. D. *J. Chem. Phys.* **1993**, 98, 5648.
- (35) Stephens, P. J.; Devlin, F. J.; Chabalowski, C. F.; Frisch, M. J. *J. Phys. Chem.* **1994**, 98, 11623.
- (36) Frisch, M. J.; Trucks, G. W.; Schlegel, H. B.; Scuseria, G. E.; Robb, M. A.; Cheeseman, J. R.; Montgomery, J. A., Jr.; Vreven, T.; Kudin, K. N.; Burant, J. C.; Millam, J. M.; Iyengar, S. S.; Tomasi, J.; Barone, V.; Mennucci, B.; Cossi, M.; Scalmani, G.; Rega, N.; Petersson, G. A.; Nakatsuji, H.; Hada, M.; Ehara, M.; Toyota, K.; Fukuda, R.; Hasegawa, J.; Ishida, M.; Nakajima, T.; Honda, Y.; Kitao, O.; Nakai, H.; Klene, M.; Li, X.; Knox, J. E.; Hratchian, H. P.; Cross, J. B.; Adamo, C.; Jaramillo, J.; Gomperts, R.; Stratmann, R. E.; Yazyev, O.; Austin, A. J.; Cammi, R.; Pomelli, C.; Ochterski, J. W.; Ayala, P. Y.; Morokuma, K.; Voth, G. A.; Salvador, P.; Dannenberg, J. J.; Zakrzewski, V. G.; Dapprich, S.; Daniels, A. D.; Strain, M. C.; Farkas, O.; Malick, D. K.; Rabuck, A. D.; Raghavachari, K.; Foresman, J. B.; Ortiz, J. V.; Cui, Q.; Baboul, A. G.; Clifford, S.; Cioslowski, J.; Stefanov, B. B.; Liu, G.; Liashenko, A.; Piskorz, P.; Komaromi, I.; Martin, R. L.; Fox, D. J.; Keith, T.; Al-Laham, M. A.; Peng, C. Y.; Nanayakkara, A.; Challacombe, M.; Gill, P. M. W.; Johnson, B.; Chen, W.; Wong, M. W.; Gonzalez, C.; Pople, J. A. *Gaussian 03*, revision C.02; Gaussian, Inc.: Pittsburgh, PA, 2003.
- (37) Mennucci, B.; Tomasi, J. *J. Chem. Phys.* **1997**, 106, 5151.
- (38) Stratmann, R. E.; Scuseria, G. E.; Frisch, M. J. *J. Chem. Phys.* **1998**, 109, 8218.
- (39) Park, H.; Zhang, K.; Ren, Y.; Nadji, S.; Sinha, N.; Taylor, S.-J.; Kang, C. *Proc. Natl. Acad. Sci. U.S.A.* **2002**, 99, 15965.
- (40) Marian, C. M.; Schneider, F.; Kleinschmidt, M.; Tatchen, J. *Eur. Phys. J. D* **2002**, 20, 357.
- (41) (a) Lhiaubet-Vallet, V.; Trzcionka, J.; Encinas, S.; Miranda, M. A.; Chouini-Lalanne, N. *J. Phys. Chem. B* **2004**, 108, 14148. (b) Chinnapen, D. J.-F.; Sen, D. *Proc. Natl. Acad. Sci. U.S.A.* **2004**, 101, 65. (c) Moysan, A.; Viari, A.; Vigny, P.; Voituriez, L.; Cadet, J.; Moustacchi, E.; Sage, E. *Biochemistry* **1991**, 30, 7080. (d) Sauvaigo, S.; Douki, T.; Odin, F.; Caillat, S.; Ravanat, J. L.; Cadet, J. *Photochem. Photobiol.* **2001**, 73, 230.